Plasma turbulence generated during particle acceleration in reconnection current sheets with magnetic islands

Q. Xia[1], V. Zharkova[1]

[1]Department of Mathematics, Physics and Electrical Engineering, Northumbria University, NE1 8ST Newcastle upon, UK

Corresponding author: Q. Xia, q.xia@northumbria.ac.uk; xiaq0207@gmail.com

Abstract

We investigate types of turbulence generated during particle acceleration in 3D Harris-type reconnecting current sheets (RCSs) with magnetic islands, using the particle-in-cell approach. When a guiding magnetic field is present in the RCS, protons and electrons become separated at ejection into the opposite semi-planes, or footpoints of reconnecting magnetic loops, due to the opposite gyration. The particles of the same charge (ions or electrons) ejected from the RCS from the opposite side where they enter called 'transit' particles. They are strongly energized and form unidirectional beams in the pitch-angle distribution. While the particles that move back to the same side where they enter the RCS are called 'bounced' particles. They gain less energy and form more diffusive pitch-angle distributions. In the RCS with magnetic islands, these two groups of particles are ejected from the X-nullpoint at the end of the islands forming the similar asymmetric distributions in the opposite separatrices. The energy difference between 'transit' and 'bounced' particles forms 'bump-on-tail' velocity distributions that naturally generate plasma turbulence. Lower-hybrid waves are generated into the magnetic islands, owing to the two-stream instabilities. The presence of the anisotropic temperature inside the RCS can introduce whistler waves. High-frequency fluctuations, upper hybrid waves or electron Bernstein waves, pile up near X-nullpoints, which are consistent with MMS observations. We present the wavelet analysis and energy spectra of the turbulent electric and magnetic field fluctuations for different frequencies. The results can be beneficial for understanding in-situ observations of energetic particles in the heliosphere with modern space missions.

1 Introduction

Magnetic reconnection is a fundamental phenomenon in plasma, during which magnetic field lines change their connectivity releasing magnetic energy in the form of wave, jets and energetic particles (Priest & Forbes, 2000; Somov, 2000). The processes of magnetic reconnection are often observed during eruptive events in the Sun (flares and coronal mass ejections (CMEs)) (Antiochos et al., 1994; Antiochos, 1998; V. V. Zharkova et al., 2011; Vilmer et al., 2011; Benz, 2017), heliospheric current sheet (V. V. Zharkova & Khabarova, 2012; Zank et al., 2014; Khabarova et al., 2015, 2017), and Earth magnetosphere (Øieroset et al., 2002; Angelopoulos et al., 2008; Chen et al., 2008). Owing to large magnetic field gradients and curvatures surrounding the reconnection sites, combined with strong gradients of the plasma temperature and density, there are large variations of the electric and magnetic fields developing inside reconnecting current sheets (RCSs) during the magnetic reconnection process (Shay et al., 2016; Xia & Zharkova, 2020).

The energetic particles generated by these processes can be detected via hard X-ray (Holman et al., 2011; V. V. Zharkova et al., 2011) and γ-ray (Vilmer et al., 2011) emission in solar flares, which are often obscured by various transport effects of particles or radiations. Much more beneficial can be obtained via in-situ observations of the heliospheric structures by WIND or ACE spacecraft, or the observations in magnetosphere current sheets (CSs) by the multi-spacecraft Magnetospheric Multiscale Mission (MMS) (Øieroset et al., 2001; Burch et al., 2016), which can measure particle distributions inside reconnecting current sheets while spacecraft passing through.

The theoretical and numerical studies of magnetic reconnection are typically performed using a simplified system of 2D anti-parallel reconnecting magnetic fields with an additional guiding magnetic field in the third dimension (2.5D approach). Such RCSs with a finite B_g are not rare in Earth magnetopause (Silin & Büchner, 2006) and flare CSs at the impulsive phase of CME eruptions (Fletcher et al., 2011). The thin elongated RCSs formed in a diffusion region between the reversed magnetic field lines are shown to often break down by tearing instability into multiple islands, or O-type nullpoints, sep-

arated by X-nullpoints (Furth et al., 1963; Bhattacharjee et al., 2009). The presence of magnetic islands in reconnecting current sheets was demonstrated by magnetohydrodynamic (Loureiro et al., 2005; Drake et al., 2006; Lapenta, 2008; Bárta et al., 2011) and kinetic simulations (Y.-M. Huang & Bhattacharjee, 2010; Karimabadi et al., 2011; Markidis et al., 2012). Such the periodic magnetic islands were often identified in many solar flares (J. Lin et al., 2005; Oka et al., 2010; Bárta et al., 2011; Takasao et al., 2012; Nishizuka et al., 2015) and coronal mass ejections (CMEs) (Song et al., 2012). Also, they are confirmed by the in-situ observations of CSs in the heliosphere (V. V. Zharkova & Khabarova, 2012; Khabarova et al., 2015) and Earth magnetotail (Zong et al., 2004; Chen et al., 2008; R. Wang et al., 2016).

In the case of full 3D RCSs, the guiding field is accepted varying in time and space. In some configurations of 3D RCSs, the out-of-plane variations of the helical magnetic structures become pretty significant, due to the kink instability, obscuring current sheet structures and making hard to define clear X-nullpoints (Daughton et al., 2011a; Egedal et al., 2012). A strong guiding field B_g can suppress the out-of-plane kink instability while leaving the concept of magnetic islands still applicable (Lapenta & Brackbill, 1997; Daughton, 1999; Cerutti et al., 2014; Sironi & Spitkovsky, 2014). Nevertheless, further studies have shown that both cases do not significantly change the scenarios of energy conversion and particle acceleration in 3D RCSs, because the dominant mechanisms of particle energisation remain the same as in the 2.5D scenario (Hesse et al., 2001; V. V. Zharkova et al., 2011; Guo et al., 2014; Dahlin et al., 2017).

Depending on magnetic field topologies, the presence of a guiding field in an RCS was revealed to cause partial or full charge separation between electrons and ions (V. V. Zharkova & Gordovskyy, 2004; Pritchett & Coroniti, 2004) due to the opposite directions of gyration based on their opposite charges. This, in turn, can lead to the preferential ejection of the oppositely charged particles into the opposite semiplanes of CSs, or opposite footpoints of reconnecting loops. It makes the hard X-ray sources to be spatially separated from the $\gamma-$ray sources in the opposite footpoints of reconnecting magnetic loops (R. P. Lin et al., 2003; Hurford et al., 2003, 2006). This charge-separation phenomenon is also confirmed in the laboratory experiments (Zhong et al., 2016). Furthermore, the separation of particles of the opposite charges introduces the polarisation electric field across the reconnection midplane, which is much larger (by two orders of magnitude) than reconnecting electric field itself (Zenitani & Hoshino, 2008; Siversky & Zharkova, 2009; Cerutti et al., 2013). The presence of polarisation electric field in RCSs has been confirmed by in-situ observations of the ion velocity profiles during the spacecraft crossings of the heliospheric CSs, which always follow the profile of polarisation electric field (V. V. Zharkova & Khabarova, 2012; V. Zharkova & Khabarova, 2015).

The neutral ambient plasmas are dragged into CSs by the magnetic diffusion process from both sides of reconnecting current ssheet. Although, entering the RCS from the opposite boundaries of a CS would also lead to different energy gains by the particles with the same charge (Siversky & Zharkova, 2009; V. V. Zharkova & Khabarova, 2012). The particles that enter an RCS from the side opposite to the that, from which they to be ejected, are classified as "transit" particles, while the particles entering the RCS from the same side where they to be ejected, are classified as "bounced" particles.

The transit particles gain significantly more energy because they become accelerated on their way to the midplane where the main acceleration occur, while bounced particles lose their energy while they approach the midplane and become gaining energy from reconnection electric field (V. V. Zharkova & Gordovskyy, 2005; Siversky & Zharkova, 2009; V. V. Zharkova & Khabarova, 2012). The energy difference between the transit and bounced particles creates particle beams with 'bump-on-tail' energy distributions, which could trigger the Buneman instability (Buneman, 1958) and generate plasma turbulence. In turn, this plasma turbulence can potentially contribute to further particle

acceleration or modify the parameters of accelerated particles (V. V. Zharkova & Agapitov, 2009; Drake et al., 2010; Muñoz & Büchner, 2016; C. Huang et al., 2017).

The target of this research is to study plasma instabilities in RCSs due to the presence of energetic particle beams extending from the X-nullpoint into magnetic islands. Because the plasma turbulence introduced by instabilities, in general, is inherently a 3D problem in realistic systems (Goldreich & Sridhar, 1995), it requires the simulation domain to be 3D. As mentioned before, the out of reconnection plane variations in 3D could obscure the CS structures, such as a clear X-nullpoint. Hence we implemented a strong B_g to the RCSs to suppress the development of the kink mode and to stabilize the magnetic island structures along the out-of-plane direction (Xia & Zharkova, 2020). Furthermore, anisotropic electric and magnetic fluctuations are expected in the presence of a local mean magnetic field $\mathbf{B}'$ (Howes et al., 2008; Boldyrev et al., 2013). Thus we will explore the variances developed both along and perpendicular to the mean magnetic field. Besides, particles have non-Maxwellian distributions in the phase space due to the developed instabilities. Ng et al. (2011) has shown that a triangular-shaped distribution could found close to the diffusion region in the electron velocity space, in which the filamentary structures correspond to different groups of particles oscillating across the RCS midplane. However, such structures would disappear outside of the diffusion region in the presence of a weak B_g (Ng et al., 2012; S. Wang et al., 2016). Thus, the implementation of a strong B_g could also help the energetic particle beams to maintain the pressure anisotropy (Le et al., 2013).

Similar to our previous study of electron pitch-angle distributions (PADs) in the RCSs (Khabarova et al., 2020; Xia & Zharkova, 2020), we intend to consider the data collected by a hypothetical spacecraft crossing the simulation domain, which allow us to analyze the electric and magnetic field fluctuations with respect to the local mean magnetic field $\mathbf{B}'$. Because the streaming instabilities can be generated in the separatrices and later extend to the exhaust region (Cattell et al., 2005; Lapenta et al., 2011; Markidis et al., 2012; Zhang et al., 2019), the positions of the virtual spacecraft are set to be in the exhaust close to the separatrices at different distances away from the X-nullpoints that form magnetic island. So we can obtain the evolution of plasma turbulence from the X-nullpoint to the O-nullpoint.

This paper is organized as follows. The magnetic field topology and the simulation model are described in section 2. The results of simulations are analyzed in section 3. A general discussion and conclusions are drawn in section 4.

2 Simulation model

To investigate turbulence generated inside RCSs with magnetic islands, let us reproduce a 3D RCS model and explore the dynamics of particles accelerated during their passage through this magnetic field topology. We used the models described in our previous papers including (Xia & Zharkova, 2020), which studied particle acceleration in coalescent and squashed magnetic islands. Similarly to (Siversky & Zharkova, 2009), the authors introduced static background electric and magnetic fields in the PIC code (Verboncoeur et al., 1995; Bowers et al., 2008). Then they followed particle acceleration and their induced electric and magnetic fields in 3D RCSs with a single or multiple X-nullpoints (magnetic islands). This approach allowed us to separate the original magnetic field configuration of the reconnection from that induced by the plasma feedback due to the accelerated particles and to discover triggers of plasma turbulence inside these complex magnetic configurations.

In the current paper, we do not separate the original and induced electromagnetic fields and adopt the self-consistent PIC simulation to investigate particle acceleration in magnetic islands generated by magnetic reconnection. We extend the 3D simulation

region to a larger domain comparing to the previous 2.5D studies by Muñoz and Büchner (2016). The simulations start with a Harris-type current sheet (CS) in the $x-z$ plane:

$$\begin{aligned} \mathbf{B}_x &= -\frac{2L_x}{L_z}\delta B_0 \sin\left(2\pi\frac{z-0.5L_z}{L_z}\right)\cos\left(\pi\frac{x}{L_x}\right), \\ \mathbf{B}_y &= B_{0y}, \\ \mathbf{B}_z &= B_{0z}\tanh\left(\frac{x}{d_{cs}}\right) + \delta B_0 \cos\left(2\pi\frac{z-0.5L_z}{L_z}\right)\sin\left(\pi\frac{x}{L_x}\right), \end{aligned} \tag{1}$$

where d_{cs} is the half thickness of RCS. The B_{0y} is the initial guiding field, which is perpendicular to the reconnection plane. In the presented simulation $b_g = B_{0y}/B_{0z} = 1.0$. The initial density variation across the CS is:

$$n = n_b + n_0\,\mathrm{sech}^2(\frac{x}{d_{cs}}). \tag{2}$$

We chose a mass ratio $m_i/m_e = 100$, a temperature ratio $T_i/T_e = 5$, a background plasma density $n_b/n_0 = 0.2$, and a frequency ratio $\omega_{pe}/\Omega_{ce} = 1.5$. The RCS initially has $d_{cs} = 0.5d_i$, where d_i is the ion inertial length. The simulation box size is $L_x \times L_y \times L_z = 51.2d_i \times 1.6d_i \times 12.8d_i$ with grid number $2048 \times 64 \times 512$ using 100 particles per cell. Along x, the conducting boundary condition for the electromagnetic field and open boundary condition for particles are used. The periodic boundary conditions are applied to both the electromagnetic field and particles along $z-$ and $y-$directions.

To trigger magnetic reconnection, let us introduce a small interruption at the beginning of the simulation, which is written in terms of $(\delta B_0...)$ in Eq. (1), where $\delta B_0 = 0.03B_{0z}$. It comes from an out-of-plane vector potential, $\delta\mathbf{B}_0 = \nabla\times\delta A_y$, where $\delta A_y \propto \cos\left(2\pi\frac{z-0.5L_z}{L_z}\right)\cos\left(\pi\frac{x}{L_x}\right)$ satisfying $\nabla\cdot\mathbf{A} = 0$. This spatial distribution helps us to set the fast reconnection to occur near the centre of the simulation box in Figure. 1(a-d), similar to that reported earlier (Daughton et al., 2011b). Multiple small magnetic islands formed, and later merged into the island across the periodic boundary as shown in the density and energy distributions of electrons in Figure. 1(c - h). The width of this crossing-boundary island increased with time. Due to the periodic boundary condition at both ends of the $z-$axis, the simulation domain represents the RCSs with a chain of magnetic islands, rather than a single X-nullpoint geometry with open exhausts. The energy distributions of electrons at $t = 24, 32\Omega_{ci}^{-1}$ show a clear asymmetry with respect to the midplane, due to the presence of the strong guiding field.

The reconnection process is still weakly affected by the kink instability at a larger time, as evidenced in the isosurface of the electron energy distribution in Figure. (2a). The distributions are similar in the different $x-z$ planes along the $y-$direction. If the guiding field is weak, the flux ropes would be strongly interrupted. For example, we observed the twist of the flux ropes in the simulation box after the same running time in the $B_g = 0$ case shown in Figure. (2b). Thus the locations and the sizes of magnetic islands, if there is any, in different $x-z$ planes would change, which makes it hard to make statistical analysis depending on the distance from the X-nullpoint on different $x-z$ planes along the $y-$direction. Therefore, we will stick to $b_g = 1$ case in the following discussions as we explained in the Introduction.

3 Simulation results

3.1 Wavenumber spectra of electromagnetic fields

During the magnetic reconnection events as shown in Figure. 1(a-h), ion-scale magnetic islands are formed in our simulations. For example, the size of the largest magnetic island reaches $\sim 36d_i$ after $t = 32\Omega_{ci}^{-1}$ in Figure. 1(g, h). It thus allows us to study the plasma turbulence developed in the downstream $> 15d_i$ from the X-nullpoint.

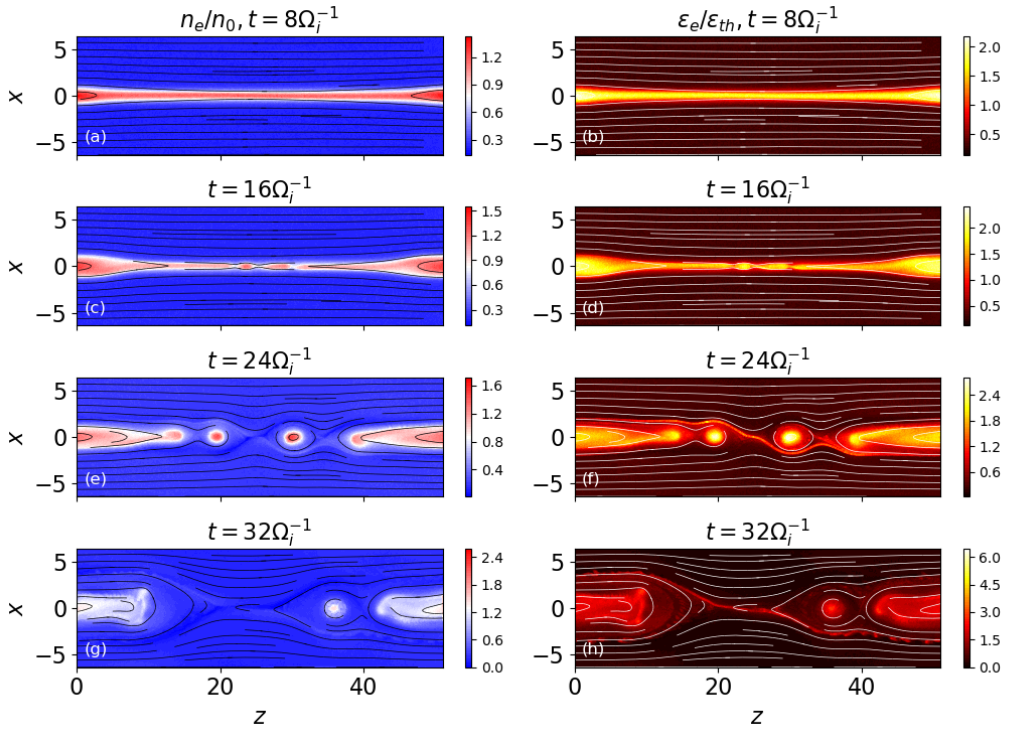

Figure 1. Density (left column) and energy (right column) distributions of electrons on the $x-z$ plane at $y=0$ at different time: (a, b) $t=8\Omega_{ci}^{-1}$, (c, d) $t=16\Omega_{ci}^{-1}$, (e, f) $t=24\Omega_{ci}^{-1}$, (g, h) $t=32\Omega_{ci}^{-1}$ for $b_g=1$.

In Figure. (3), the power spectrum of electric (magnetic) fields of the whole box are measured at $t=32\Omega_{ci}^{-1}$ as $|\mathbf{E}|^2(k)$ ($|\mathbf{B}|^2(k)$) in the Fourier space, where k stands for the wavenumber in the reconnection plane. In this session, we did not discuss the anisotropic problem ($k_\parallel$, $k_\perp$ to the local magnetic field) in this session, because there is no uniform background magnetic field across the domain as studied in homogeneous plasma turbulence problem, where the local magnetic field $\mathbf{B}(x,y,z) \approx \mathbf{B}' + \delta\mathbf{B}(x,y,z)$ (Goldreich & Sridhar, 1995).

In this model, the wave-number spectrum of the magnetic field formed a quasi-stable range from $kd_i = 1$ down to above $kd_e = 1$. A least square fitting of $|\mathbf{B}|^2(k) \propto k^\alpha$ over this range indicates the slope $\alpha \approx -2.7$. The spectrum of the electric fields drops significantly at scales near the electron inertial scale (the solid line, $k_{d_e}(n_0)$, and dashed line, $k_{d_e}(n_b)$, on the right side of the spectra are calculated from the RCS density and background density). It suggests that during the selected time the large-scale waves are quasi-stable. Meanwhile, the spectra show that the electromagnetic energy is strongly damped at the electron characteristic scale.

3.2 Phase space distributions

As soon as particles became accelerated and were ejected from the X-nullpoint, they form the beams with different energies defined by the difference in energy gains of transit and bounced particles (Xia & Zharkova, 2020) forming 'bump-on-tail' energy distributions. These beams with two-peak energy distributions can naturally trigger Buneman instabilities. In addition, highly anisotropic energy distributions in the beams, and

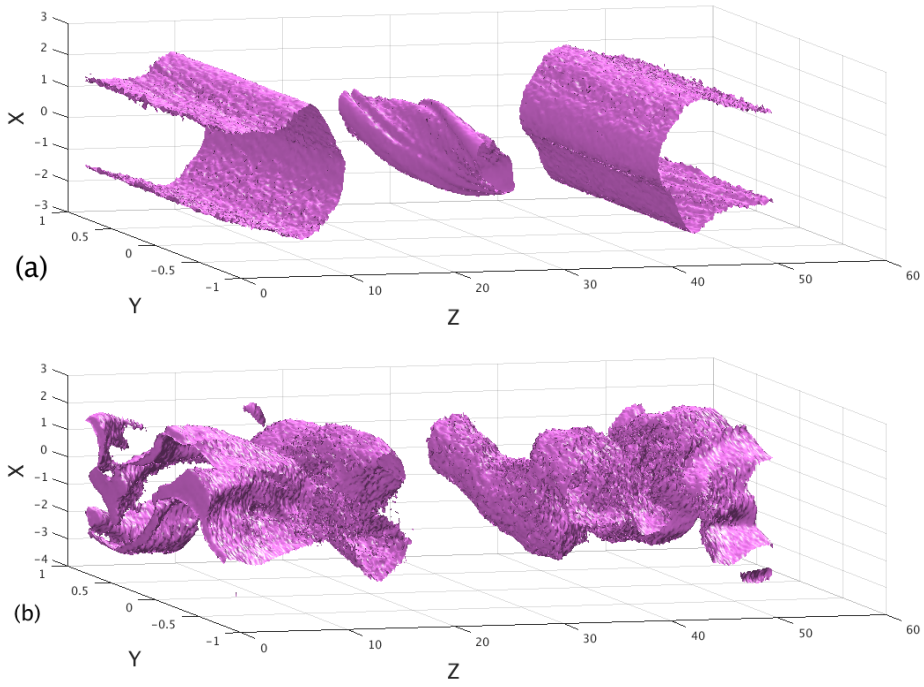

Figure 2. *Upper plot*: Isosurface of the electron energy distribution (the 35% contour of the max energy) in the simulation box of Figure. (1) at $t = 28\Omega_{ci}^{-1}$. *Bottom plot*: Isosurface of the electron energy distribution after the same running time from a similar simulation using $b_g = 0$.

the presence of a large density gradient between the beams and ambient plasma would introduce other instabilities, which tend to prevent beams from propagating as beams and generate plasma turbulence.

We examined the changes in the $v_y - x$ phase space for both ions and electrons along the cuts perpendicular to the reconnection midplane at different distances away from the X-nullpoint as shown in Figure 4. The non-Maxwellian feature first showed up in Figure 4(c): at $z = 15$ (or $\Delta z \sim 7$ away from the main X-nullpoint), electron holes are formed in the phase space near $x = -1.5$ to 1.0, which is triggered by the beam-driven lower hybrid instability.

Then as the inspecting plane moves deeper into the magnetic island, the perturbation in the ion phase space was found at $z = 10$ (or$\Delta z \sim 12$ away from the X-nullpoint) in Figure 4(b), where the arcs in the $x = 0$ to 2 region represent different groups of ion beams. We did not find any clear ion holes in the phase space, but those arcs disappear quickly further in the downstream, which suggest the ion beams are also suppressed by plasma turbulence.

3.3 Frequency analysis

3.3.1 Wavelet analysis

The plasma turbulence introduced by beam instabilities can also be studied using electric and magnetic fluctuations in the frequency domain. After we identified the instability signals in the particle phase space, we took the advantage of wavelet analysis,

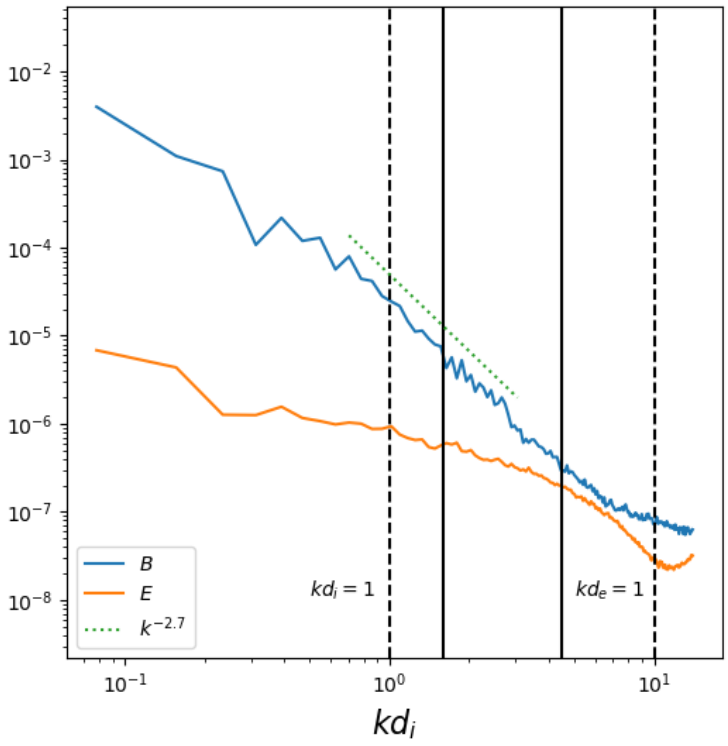

Figure 3. Power spectra of the electric (normalized by $B_0^2 V_A^2$) and magnetic fields (normalized by B_0^2). The wave vector is normalized to d_i^{-1} of n_0. The corresponding $k_{d_i}(n_0)$, $k_{d_e}(n_0)$ are marked in dash lines. The solid lines indicate the ion gyroscale $k_{\rho_i}^{-1}$ (left) and electron inertial scale calculated by the background density $k_{d_e}(n_b)^{-1}$ (right).

which is a powerful tool to analyse time-series data collected by a pinpoint in the domain, to study the fluctuations using discrete wavelet transform (Farge, 1992).

We explored the fluctuations of electric and magnetic fields in the exhaust obtained during the acceleration of particles in the RCS. The signals at different grids along the $y-$direction were transformed to wavelet power spectra using Morlet wavelet. Then the results were averaged along the out-of-plane $y-$axis. The wavelet power spectra of both electric and magnetic field components shared the same features. For example, Figure. (5) shows the results using the data of the B_x component recorded at point B ($z = 15, x = 0.25$, where the electron holes were observed in the phase space in Figure. 4(c)) for a period of $5\Omega_{ci}^{-1}$.

Comparing to the wavenumber spectra of electromagnetic fields from the whole region (section 3.1), the wavelet analysis showed that the dominant fluctuations have long periods (or low-frequency, $\ll \Omega_{ce}$). Furthermore, the wavelet transform revealed richer features in the high-frequency region. Figure. (4) depicts several high-frequency signals represented by dark purple stripes, which reached electron characteristic frequency. Thus, the electromagnetic fields spectra in wavenumber and via wavelet transform both indicate the important role of electrons in plasma turbulence developed in magnetic islands.

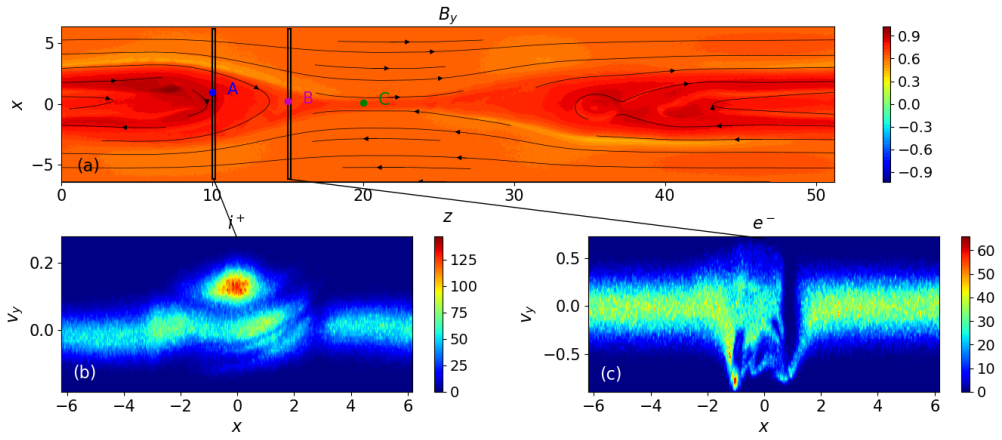

Figure 4. Phase-space distribution functions of the (b) ions and (c) electrons at difference locations at $t = 36\Omega_i^{-1}$. The out-of-plane magnetic field component B_y at $y = 0$ is coloured in panel (a) with the in-plane magnetic field topology (black solid lines). The electromagnetic fields at A, B, and C are recorded for further analysis. The phase space structures in (b) and (c) are captured in the vertically elongated boxes with a width of $\Delta y = 0.2d_i$. The main X-nullpoint is located at $z = 22, x = 0$. This simulation started with a strong guiding field ($b_g = 1$).

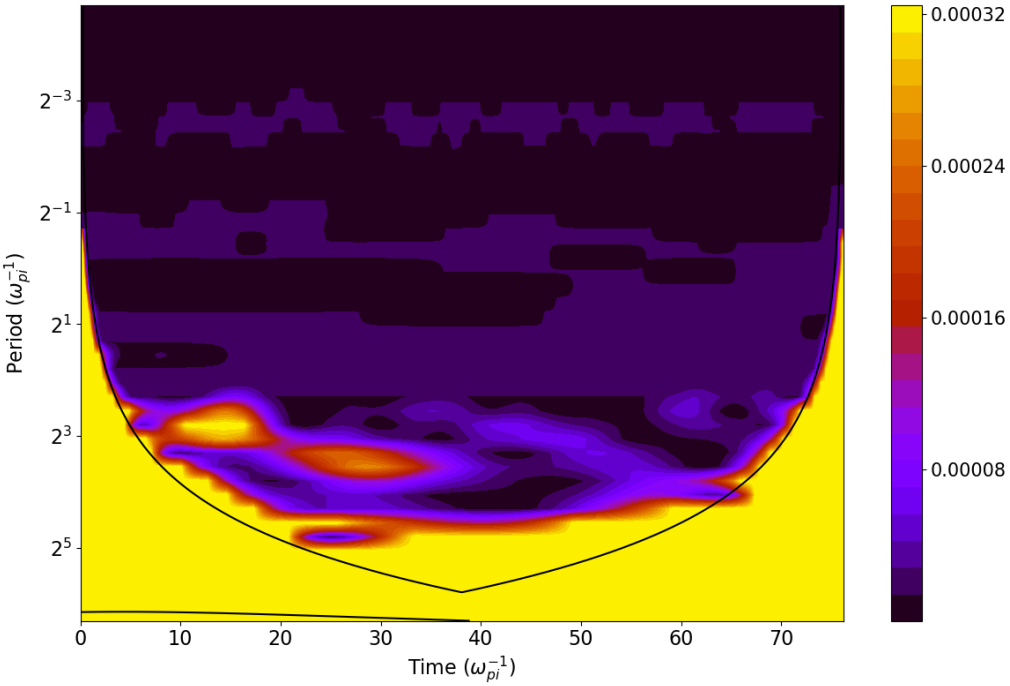

Figure 5. Local wavelet power spectrum of B_x (the purple point B at $z = 15, x = 0.25$ in Figure. 4) of the time series of B_x components, using Morlet wavelet. The solid dark curve encloses the regions of $> 95\%$ confidence.

3.3.2 Frequency spectra of electromagnetic fields

Furthermore, let us split now the electric and magnetic fields to the parallel and perpendicular components based on the local mean magnetic field $\mathbf{B}'$. This idea comes

from plasma turbulence concepts that fluctuations exhibit anisotropic features in the presence of a strong background field (sometimes also called the guide field, but it is different from the concept of the guiding field B_g in magnetic reconnection). In this section, this local mean magnetic field was averaged over both the space and the time: the surveyed box size was $\Delta L_x(=0.2d_i)\times L_y\times\Delta L_z(=0.2d_i)$ surrounding the selected points in Figure. (4); the values were also averaged over $5\Omega_{ci}^{-1}$ period of simulation time. Then the $\mathbf{B}$ and $\mathbf{E}$ components on every grid are projected to this $\mathbf{B}'$ to get the parallel and perpendicular components. The the results in Figure. (6) were averaged over the Fourier spectra of the electric and magnetic field components from the surveyed grid points.

In this session, we assumed virtual spacecraft staying at three different locations: A, B, and C as shown in Figure. 4. From point C $\rightarrow$ A, the selected points are further away from the X-nullpoint. The most obvious changes are in the low-frequency part: right below Ω_{ce}, we could find large enhancement in the amplitude of $B_\perp$ (and a spike in $E_\parallel$), which could contribute to the generation of whistler waves in the region near points A and B. Further down in the lower frequency region, the amplitudes of $B_\parallel$, $B_\perp$, and $E_\perp$ are much larger over a large range. The small bump near ω_{lh} (especially in the electric fields near point A at $z=10, x=1$) represent the lower hybrid waves.

In the very-high-frequency part ($\geq\omega_{pe}$), we first noticed that the perpendicular electric field $E_\perp$ at $f>\omega_{pe}$ is damped significantly as it moves away from the X-nullpoint. In other words, these waves represented by $E_\perp$ are only observable near X-nullpoints. Furthermore, both high-frequency fluctuations of $\delta\mathbf{E}$ and $\delta\mathbf{B}$ are mainly perpendicular to $\mathbf{B}'$. Further analysis of the fluctuations on the perpendicular plane showed that $E_\perp, B_\perp$ are right-hand polarized, which are consistent with electron circular direction in the plane. In the sub-high-frequency region, $\Omega_{ce}<f<\omega_{pe}$, we found several distinct spikes in all the fields at three locations. Considering that the periodic boundary condition along $z-$axis stands for simulating a chain of magnetic islands, it suggests that the magnetic island pool is fulfilled with these electromagnetic fluctuations above Ω_{ce}. Besides, we also noticed that the enhancement near $f\approx\omega_{lh}$, $f<\Omega_{ce}$, and $\Omega_{ce}<f<\omega_{pe}$ are consistent with the dark horizontal stripes in the wavelet power spectrum in Figure. (5). By splitting the electromagnetic fluctuations into the parallel and perpendicular direction, here we further identified the differences between those stripe signals appeared in the wavelet analysis.

4 Discussion and Conclusions

In this paper, we simulated 3D RCSs with magnetic islands generated from a Harris-type CS equilibrium. Our goal was to track the plasma turbulence development following the ejection of energetic particles in magnetic islands, from the X-nullpoint to the O-nullpoint. This can provide more signatures for us to identify RCS structures, which is a challenging problem in space plasma due to the limited opportunities of spontaneous multiple spacecraft observation within a single RCS. In our previous study, we have studied the pitch-angle distributions of electrons and found characteristic signals, such as counter-streaming strahls and heat flux dropouts, which depends on the specific magnetic field topology (Khabarova et al., 2020; Xia & Zharkova, 2020). Here we shift our attention to the electric and magnetic field fluctuations in the frequency domain, with growing interests and available data in the community.

Particles that drift into the RCSs from opposite boundaries would gain different energy gains in the presence of a magnetic guiding field Siversky and Zharkova (2009). Previous 2.5D PIC simulation by Siversky and Zharkova (2009) of particle acceleration near a single X-nullpoint have shown these accelerated particle beams with different energies form a bump-on-tail distribution at the ejection, which leads to Buneman instabilities (Buneman, 1958) and generates turbulence (Jaroschek et al., 2004; Siversky & Zharkova, 2009; Drake et al., 2010). Later Muñoz and Büchner (2016) showed that non-

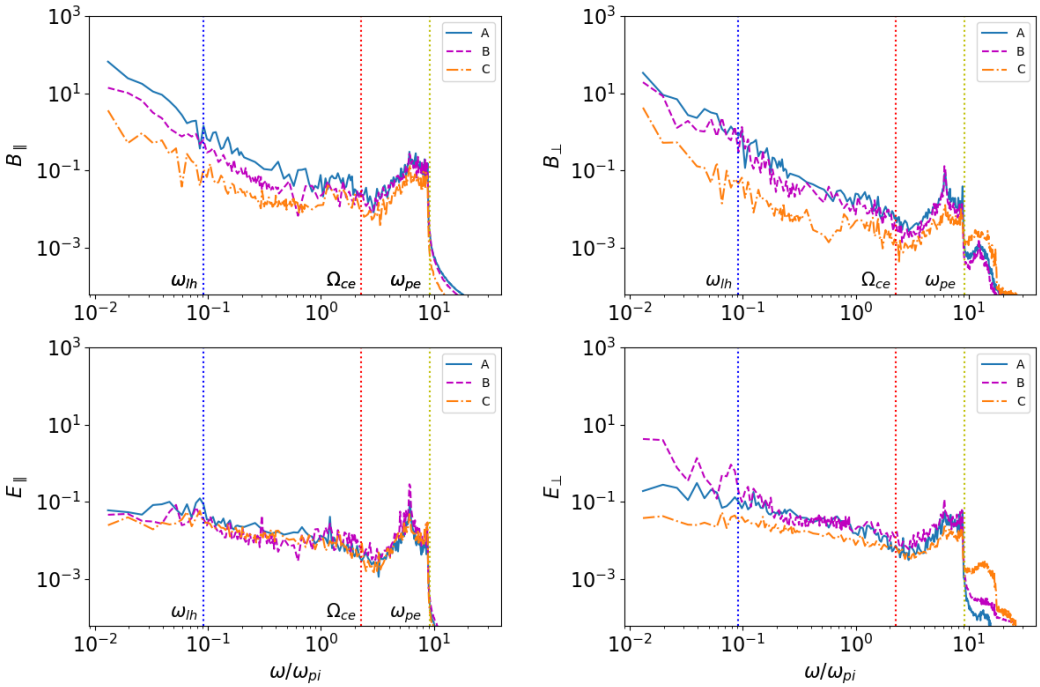

Figure 6. The spectra of different **E** and **B** components at selected points (marked in corresponding colors in Figure. 4) as functions of the frequency (normalized to ω_{pi}): $B_\parallel$, $E_\parallel$, $B_\perp$, $E_\perp$ with respect to the local mean magnetic field in $3D$. The characteristic lower-hybrid frequency ω_{lh}, electron gyro frequency Ω_{ce}, and electron plasma frequency ω_{pe} are labelled as vertical dotted lines.

Maxwellian distributions appeared in the electron phase space at a distance $\sim 6d_i$ away from the X-nullpoint, generating lower hybrid waves. Therefore, we set a larger 3D simulation domain, in which magnetic reconnection generated a large magnetic island with size $\sim 32d_i$. A strong guiding field B_g is implemented to suppress the kink instability and keep the geometry quasi-similar on each $x-z$ plane. It allows us to get statistical results by averaging the data collected from 64 grid points along the $y-$direction.

In this large 3D simulation box, the turbulent magnetic field in the RCS formed a steady spectral slope $\propto k^{-2.7}$ near the ion inertial length, and a steeper cascade at electron scales at $t = 36\Omega_{ci}^{-1}$, which is consistent with the other 3D PIC simulations(Karimabadi et al., 2013; X. Li et al., 2019), suggesting quasi-stable turbulence is built up at this moment. Hence we inspected the phase space of particles at this selected time, and identified two regions with clear non-Maxwellian distributions: the electron beams evolved into phase-space holes $\sim 7d_i$ away from the main X-nullpoint, which indicates that streaming instabilities broke the beam structures. This was consistent with the previous numerical findings (Drake et al., 2003; Muñoz & Büchner, 2016) and observations in the Earth's magnetotail (Khotyaintsev et al., 2010). Furthermore, we also that found the arc-shape distributions, which represent different ion beams, showed up in the phase space at $12d_i$ from the X-nullpoint and disappeared shortly in the further downstream. Thus the ion beams would also be quickly suppressed by two-stream instabilities. The difference between the electron and ion phase space suggests that to understand the full picture of plasma turbulence due to magnetic reconnection, it requires the simulation size to be much bigger than the diffusion region (Eastwood et al., 2018; Zhang et al., 2019).

By analysis the changes of the electric and magnetic fields at different locations, we could connect these non-Maxwellian features with distinct fluctuations. The electric and magnetic field information collected by a virtual spacecraft between the X-nullpoint and the O-nullpoint were transformed to the frequency domain. The wavelet power spectrum in the exhaust showed that low-frequency fluctuations dominate the region. Several distinct groups of fluctuations with higher frequencies could be identified within the surveyed period. Because of the anisotropy of plasma turbulence in the presence of a strong magnetic field (Boldyrev et al., 2013; Loureiro, Nuno F. & Boldyrev, Stanislav, 2017), we compared the parallel and perpendicular components of the electric and magnetic field data separately. These data are collected by three virtual spacecraft, which are positioned from near X-nullpoint to deep in the exhaust region.

The electron beams are found to introduce high-frequency electromagnetic fluctuations above Ω_{ce}, which are observed through all of the three surveyed points in Figure. (3). These fluctuations spread from the electron gyro frequency to upper hybrid frequency. Similar signals are found in the inflow region close to the X-nullpoint rather than the exhaust by Lapenta et al. (2020). It suggests that these high-frequency harmonic signals could result from the periodic boundary condition, which represents a region filled with magnetic island structures in the RCS. It thus prevents the waves from escaping to the open field regions.

Such high-frequency harmonics above Ω_{ce} have recently been discovered by MMS satellites near the electron diffusion region in the magnetopause (Dokgo et al., 2019). The authors identified these high-frequency fluctuations as the harmonics of upper hybrid waves, although they exhibited electromagnetic features. On the other hand, W. Y. Li et al. (2020) reported the signals in $E_\perp$ and $B_\perp$ power spectra peak at the harmonics of $n\Omega_{ce}$, where $n = 1, 2, 3, ...$ near an electron diffusion region in the magnetotail. Thus they are contributed to electron Bernstein waves. One difference in the observation is that $\omega_{pe}/\Omega_{ce} \approx 27$ in the magnetosphere, which keeps those two signals well separated. But this ratio is much low in most PIC simulations (here it is 3.5) so we could not distinguish them clearly.

The frequency spectra of electric and magnetic fields obtained at different locations also revealed that turbulence was changing in the outflow from the X-nullpoint to O-nullpoint. The ultra-high frequency electrostatic fluctuations in the $E_\perp$ component, e.g. the high harmonics of electron Bernstein waves (Bernstein, 1958; Gusakov & Surkov, 2007), were found to only exist near the X-nullpoint. This is consistent with the MMS observations mentioned above. As the observer moved away from the X-nullpoint, the whistler waves were developing into peaks near the sub-Ω_{ce} (Fujimoto & Sydora, 2008; Muñoz & Büchner, 2016; Graham et al., 2016). These waves could be generated by the temperature anisotropic instabilities (Gary & Karimabadi, 2006) and are also consistent with the electron holes in the phase space (Goldman et al., 2014). Meanwhile, low-frequency waves dominated the regions further in the outflow. The amplitudes of the fluctuations increased near the lower-hybrid frequency (Rogers et al., 2000). The lower-hybrid waves could be generated by two-stream instabilities as shown in the energy distribution of Figure. (2b) (Papadopoulos & Palmadesso, 1976; Zhou et al., 2014; Xia & Zharkova, 2020), or due to the strong density gradient near the separatrices and in the outflow (Scholer et al., 2003; Divin et al., 2015).

In summary, we have identified the plasma turbulence in the RCS with magnetic islands and linked the characteristic fluctuations to the non-Maxwellian distributions of particles in phase space. The observed waves vary as a function of the distance away from the X-nullpoint. The high-frequency perpendicular fluctuations damp quickly out of the electron diffusion region, and the lower-frequency whistler and lower-hybrid waves are developing because of the streaming instabilities and strong plasma temperature anisotropy and density gradient. These signals offer new observational evidence of the existing of local particle acceleration due to magnetic reconnection in the solar wind. These works

potentially benefit the in-situ study of RCSs near the Sun from Parker Solar Probe (Phan et al., 2020).

Acknowledgments

The authors acknowledge the funding for this research provided by the U.S. Air Force grant *PRJ02156*. This work used the DiRAC Complexity system, operated by the University of Leicester IT Services, which forms part of the STFC DiRAC HPC Facility (*www.dirac.ac.uk*). This equipment is funded by BIS National E-Infrastructure capital grant ST/K000373/1 and STFC DiRAC Operations grant ST/K0003259/1. DiRAC is part of the National e-Infrastructure.

References

Angelopoulos, V., McFadden, J. P., Larson, D., Carlson, C. W., Mende, S. B., Frey, H., ... Kepko, L. (2008, August). Tail Reconnection Triggering Substorm Onset. *Science*, *321*, 931. doi: 10.1126/science.1160495

Antiochos, S. K. (1998, August). The Magnetic Topology of Solar Eruptions. *Astrophysical Journal, Letters*, *502*, L181-L184. doi: 10.1086/311507

Antiochos, S. K., Dahlburg, R. B., & Klimchuk, J. A. (1994, January). The magnetic field of solar prominences. *Astrophysical Journal, Letters*, *420*, L41-L44. doi: 10.1086/187158

Bárta, M., Büchner, J., Karlický, M., & Skála, J. (2011, August). Spontaneous Current-layer Fragmentation and Cascading Reconnection in Solar Flares. I. Model and Analysis. *Astrophysical Journal*, *737*, 24. doi: 10.1088/0004-637X/737/1/24

Benz, A. O. (2017, December). Flare Observations. *Living Reviews in Solar Physics*, *14*, 2. doi: 10.1007/s41116-016-0004-3

Bernstein, I. B. (1958, January). Waves in a Plasma in a Magnetic Field. *Physical Review*, *109*(1), 10-21. doi: 10.1103/PhysRev.109.10

Bhattacharjee, A., Huang, Y.-M., Yang, H., & Rogers, B. (2009). Fast reconnection in high-lundquist-number plasmas due to the plasmoid instability. *Physics of Plasmas*, *16*(11), 112102. Retrieved from `https://doi.org/10.1063/1.3264103` doi: 10.1063/1.3264103

Boldyrev, S., Horaites, K., Xia, Q., & Perez, J. C. (2013, November). Toward a Theory of Astrophysical Plasma Turbulence at Subproton Scales. *Astrophysical Journal*, *777*(1), 41. doi: 10.1088/0004-637X/777/1/41

Bowers, K. J., Albright, B. J., Yin, L., Bergen, B., & Kwan, T. J. T. (2008, May). Ultrahigh performance three-dimensional electromagnetic relativistic kinetic plasma simulationa). *Physics of Plasmas*, *15*, 055703. doi: 10.1063/1.2840133

Buneman, O. (1958, Jul). Instability, turbulence, and conductivity in current-carrying plasma. *Phys. Rev. Lett.*, *1*, 8–9. Retrieved from `https://link.aps.org/doi/10.1103/PhysRevLett.1.8` doi: 10.1103/PhysRevLett.1.8

Burch, J. L., Moore, T. E., Torbert, R. B., & Giles, B. L. (2016, March). Magnetospheric Multiscale Overview and Science Objectives. *Space Science Reviews*, *199*(1-4), 5-21. doi: 10.1007/s11214-015-0164-9

Cattell, C., Dombeck, J., Wygant, J., Drake, J. F., Swisdak, M., Goldstein, M. L., ... Balogh, A. (2005). Cluster observations of electron holes in association with magnetotail reconnection and comparison to simulations. *Journal of Geophysical Research: Space Physics*, *110*(A1). Retrieved from `https://agupubs.onlinelibrary.wiley.com/doi/abs/10.1029/2004JA010519` doi: 10.1029/2004JA010519

Cerutti, B., Werner, G. R., Uzdensky, D. A., & Begelman, M. C. (2013, June). Simulations of Particle Acceleration beyond the Classical Synchrotron Burnoff Limit in Magnetic Reconnection: An Explanation of the Crab Flares. *Astro-*

physical Journal, *770*(2), 147. doi: 10.1088/0004-637X/770/2/147

Cerutti, B., Werner, G. R., Uzdensky, D. A., & Begelman, M. C. (2014, February). Three-dimensional Relativistic Pair Plasma Reconnection with Radiative Feedback in the Crab Nebula. *Astrophysical Journal*, *782*(2), 104. doi: 10.1088/0004-637X/782/2/104

Chen, L.-J., Bhattacharjee, A., Puhl-Quinn, P. A., Yang, H., Bessho, N., Imada, S., ... Georgescu, E. (2008, January). Observation of energetic electrons within magnetic islands. *Nature Physics*, *4*, 19-23. doi: 10.1038/nphys777

Dahlin, J. T., Drake, J. F., & Swisdak, M. (2017, September). The role of three-dimensional transport in driving enhanced electron acceleration during magnetic reconnection. *Physics of Plasmas*, *24*(9), 092110. doi: 10.1063/1.4986211

Daughton, W. (1999, April). The unstable eigenmodes of a neutral sheet. *Physics of Plasmas*, *6*(4), 1329-1343. doi: 10.1063/1.873374

Daughton, W., Roytershteyn, V., Karimabadi, H., Yin, L., Albright, B. J., Bergen, B., & Bowers, K. J. (2011a, July). Role of electron physics in the development of turbulent magnetic reconnection in collisionless plasmas. *Nature Physics*, *7*, 539-542. doi: 10.1038/nphys1965

Daughton, W., Roytershteyn, V., Karimabadi, H., Yin, L., Albright, B. J., Bergen, B., & Bowers, K. J. (2011b, July). Role of electron physics in the development of turbulent magnetic reconnection in collisionless plasmas. *Nature Physics*, *7*, 539-542. doi: 10.1038/nphys1965

Divin, A., Khotyaintsev, Y. V., Vaivads, A., André, M., Markidis, S., & Lapenta, G. (2015, April). Evolution of the lower hybrid drift instability at reconnection jet front. *Journal of Geophysical Research (Space Physics)*, *120*(4), 2675-2690. doi: 10.1002/2014JA020503

Dokgo, K., Hwang, K.-J., Burch, J. L., Choi, E., Yoon, P. H., Sibeck, D. G., & Graham, D. B. (2019, July). High-Frequency Wave Generation in Magnetotail Reconnection: Nonlinear Harmonics of Upper Hybrid Waves. *Geophysics Research Letters*, *46*(14), 7873-7882. doi: 10.1029/2019GL083361

Drake, J. F., Opher, M., Swisdak, M., & Chamoun, J. N. (2010, February). A Magnetic Reconnection Mechanism for the Generation of Anomalous Cosmic Rays. *Astrophysical Journal*, *709*, 963-974. doi: 10.1088/0004-637X/709/2/963

Drake, J. F., Swisdak, M., Cattell, C., Shay, M. A., Rogers, B. N., & Zeiler, A. (2003). Formation of electron holes and particle energization during magnetic reconnection. *Science*, *299*(5608), 873–877. Retrieved from `https://science.sciencemag.org/content/299/5608/873` doi: 10.1126/science.1080333

Drake, J. F., Swisdak, M., Che, H., & Shay, M. A. (2006, October). Electron acceleration from contracting magnetic islands during reconnection. *Nature*, *443*, 553-556. doi: 10.1038/nature05116

Eastwood, J. P., Mistry, R., Phan, T. D., Schwartz, S. J., Ergun, R. E., Drake, J. F., ... Russell, C. T. (2018). Guide field reconnection: Exhaust structure and heating. *Geophysical Research Letters*, *45*(10), 4569-4577. Retrieved from `https://agupubs.onlinelibrary.wiley.com/doi/abs/10.1029/2018GL077670` doi: 10.1029/2018GL077670

Egedal, J., Daughton, W., & Le, A. (2012, April). Large-scale electron acceleration by parallel electric fields during magnetic reconnection. *Nature Physics*, *8*, 321-324. doi: 10.1038/nphys2249

Farge, M. (1992). Wavelet transforms and their applications to turbulence. *Annual Review of Fluid Mechanics*, *24*(1), 395-458. Retrieved from `https://doi.org/10.1146/annurev.fl.24.010192.002143` doi: 10.1146/annurev.fl.24.010192.002143

Fletcher, L., Dennis, B. R., Hudson, H. S., Krucker, S., Phillips, K., Veronig, A., ... Temmer, M. (2011, September). An Observational Overview of Solar Flares.

Space Science Reviews, *159*(1-4), 19-106. doi: 10.1007/s11214-010-9701-8

Fujimoto, K., & Sydora, R. D. (2008, October). Whistler waves associated with magnetic reconnection. *Geophysics Research Letters*, *35*(19), L19112. doi: 10.1029/2008GL035201

Furth, H. P., Killeen, J., & Rosenbluth, M. N. (1963, April). Finite-Resistivity Instabilities of a Sheet Pinch. *Physics of Fluids*, *6*(4), 459-484. doi: 10.1063/1.1706761

Gary, S. P., & Karimabadi, H. (2006, November). Linear theory of electron temperature anisotropy instabilities: Whistler, mirror, and Weibel. *Journal of Geophysical Research (Space Physics)*, *111*(A11), A11224. doi: 10.1029/2006JA011764

Goldman, M. V., Newman, D. L., Lapenta, G., Andersson, L., Gosling, J. T., Eriksson, S., ... Ergun, R. (2014, April). Čerenkov Emission of Quasiparallel Whistlers by Fast Electron Phase-Space Holes during Magnetic Reconnection. *Physical Review Letters*, *112*(14), 145002. doi: 10.1103/PhysRevLett.112.145002

Goldreich, P., & Sridhar, S. (1995, January). Toward a Theory of Interstellar Turbulence. II. Strong Alfvenic Turbulence. *Astrophysical Journal*, *438*, 763. doi: 10.1086/175121

Graham, D. B., Vaivads, A., Khotyaintsev, Y. V., & Andr, M. (2016). Whistler emission in the separatrix regions of asymmetric magnetic reconnection. *Journal of Geophysical Research: Space Physics*, *121*(3), 1934-1954. Retrieved from `https://agupubs.onlinelibrary.wiley.com/doi/abs/10.1002/2015JA021239` doi: 10.1002/2015JA021239

Guo, F., Li, H., Daughton, W., & Liu, Y.-H. (2014, October). Formation of Hard Power Laws in the Energetic Particle Spectra Resulting from Relativistic Magnetic Reconnection. *Physical Review Letters*, *113*(15), 155005. doi: 10.1103/PhysRevLett.113.155005

Gusakov, E. Z., & Surkov, A. V. (2007, May). Induced backscattering in an inhomogeneous plasma at the upper hybrid resonance. *Plasma Physics and Controlled Fusion*, *49*(5), 631-639. doi: 10.1088/0741-3335/49/5/005

Hesse, M., Kuznetsova, M., & Birn, J. (2001, December). Particle-in-cell simulations of three-dimensional collisionless magnetic reconnection. *Journal of Geophysics Research*, *106*, 29831-29842. doi: 10.1029/2001JA000075

Holman, G. D., Aschwanden, M. J., Aurass, H., Battaglia, M., Grigis, P. C., Kontar, E. P., ... Zharkova, V. V. (2011, September). Implications of X-ray Observations for Electron Acceleration and Propagation in Solar Flares. *Space Science Reviews*, *159*, 107-166. doi: 10.1007/s11214-010-9680-9

Howes, G. G., Dorland, W., Cowley, S. C., Hammett, G. W., Quataert, E., Schekochihin, A. A., & Tatsuno, T. (2008, February). Kinetic Simulations of Magnetized Turbulence in Astrophysical Plasmas. *Physical Review Letters*, *100*(6), 065004. doi: 10.1103/PhysRevLett.100.065004

Huang, C., Lu, Q., Wang, R., Guo, F., Wu, M., Lu, S., & Wang, S. (2017, feb). Development of turbulent magnetic reconnection in a magnetic island. *The Astrophysical Journal*, *835*(2), 245. Retrieved from `https://doi.org/10.3847%2F1538-4357%2F835%2F2%2F245` doi: 10.3847/1538-4357/835/2/245

Huang, Y.-M., & Bhattacharjee, A. (2010). Scaling laws of resistive magnetohydrodynamic reconnection in the high-lundquist-number, plasmoid-unstable regime. *Physics of Plasmas*, *17*(6), 062104. Retrieved from `https://doi.org/10.1063/1.3420208` doi: 10.1063/1.3420208

Hurford, G. J., Krucker, S., Lin, R. P., Schwartz, R. A., Share, G. H., & Smith, D. M. (2006, June). Gamma-Ray Imaging of the 2003 October/November Solar Flares. *Astrophysical Journal, Letters*, *644*, L93-L96. doi: 10.1086/505329

Hurford, G. J., Schwartz, R. A., Krucker, S., Lin, R. P., Smith, D. M., & Vilmer, N. (2003, October). First Gamma-Ray Images of a Solar Flare. *Astrophysical*

Journal, Letters, *595*, L77-L80. doi: 10.1086/378179

Jaroschek, C. H., Treumann, R. A., Lesch, H., & Scholer, M. (2004, March). Fast reconnection in relativistic pair plasmas: Analysis of particle acceleration in self-consistent full particle simulations. *Physics of Plasmas*, *11*(3), 1151-1163. doi: 10.1063/1.1644814

Karimabadi, H., Dorelli, J., Roytershteyn, V., Daughton, W., & Chacón, L. (2011, July). Flux Pileup in Collisionless Magnetic Reconnection: Bursty Interaction of Large Flux Ropes. *Physical Review Letters*, *107*(2), 025002. doi: 10.1103/PhysRevLett.107.025002

Karimabadi, H., Roytershteyn, V., Daughton, W., & Liu, Y.-H. (2013, October). Recent Evolution in the Theory of Magnetic Reconnection and Its Connection with Turbulence. *Space Science Reviews*, *178*(2-4), 307-323. doi: 10.1007/s11214-013-0021-7

Khabarova, O., Zank, G. P., Li, G., le Roux, J. A., Webb, G. M., Dosch, A., & Malandraki, O. E. (2015, August). Small-scale Magnetic Islands in the Solar Wind and Their Role in Particle Acceleration. I. Dynamics of Magnetic Islands Near the Heliospheric Current Sheet. *Astrophysical Journal*, *808*, 181. doi: 10.1088/0004-637X/808/2/181

Khabarova, O., Zharkova, V., Xia, Q., & Malandraki, O. E. (2020, may). Counterstreaming strahls and heat flux dropouts as possible signatures of local particle acceleration in the solar wind. *The Astrophysical Journal*, *894*(1), L12. Retrieved from `https://doi.org/10.3847%2F2041-8213%2Fab8cb8` doi: 10.3847/2041-8213/ab8cb8

Khabarova, O. V., Zank, G. P., Malandraki, O. E., Li, G., le Roux, J. A., & Webb, G. M. (2017, January). Observational evidence for local particle acceleration associated with magnetically confined magnetic islands in the heliosphere - a review. *Sun and Geosphere*, *12*, 23-30.

Khotyaintsev, Y. V., Vaivads, A., André, M., Fujimoto, M., Retinò, A., & Owen, C. J. (2010, Oct). Observations of slow electron holes at a magnetic reconnection site. *Phys. Rev. Lett.*, *105*, 165002. Retrieved from `https://link.aps.org/doi/10.1103/PhysRevLett.105.165002` doi: 10.1103/PhysRevLett.105.165002

Lapenta, G. (2008, June). Self-Feeding Turbulent Magnetic Reconnection on Macroscopic Scales. *Physical Review Letters*, *100*(23), 235001. doi: 10.1103/PhysRevLett.100.235001

Lapenta, G., & Brackbill, J. U. (1997, December). A kinetic theory for the drift-kink instability. *Journal of Geophysics Research*, *102*(A12), 27099-27108. doi: 10.1029/97JA02140

Lapenta, G., Markidis, S., Divin, A., Goldman, M. V., & Newman, D. L. (2011, September). Bipolar electric field signatures of reconnection separatrices for a hydrogen plasma at realistic guide fields. *Geophysics Research Letters*, *38*(17), L17104. doi: 10.1029/2011GL048572

Lapenta, G., Pucci, F., Goldman, M. V., & Newman, D. L. (2020, January). Local Regimes of Turbulence in 3D Magnetic Reconnection. *Astrophysical Journal*, *888*(2), 104. doi: 10.3847/1538-4357/ab5a86

Le, A., Egedal, J., Ohia, O., Daughton, W., Karimabadi, H., & Lukin, V. S. (2013, Mar). Regimes of the electron diffusion region in magnetic reconnection. *Phys. Rev. Lett.*, *110*, 135004. Retrieved from `https://link.aps.org/doi/10.1103/PhysRevLett.110.135004` doi: 10.1103/PhysRevLett.110.135004

Li, W. Y., Graham, D. B., Khotyaintsev, Y. V., Vaivads, A., André, M., Min, K., ... Burch, J. L. (2020, January). Electron Bernstein waves driven by electron crescents near the electron diffusion region. *Nature Communications*, *11*, 141. doi: 10.1038/s41467-019-13920-w

Li, X., Guo, F., Li, H., Stanier, A., & Kilian, P. (2019, October). Formation of Power-law Electron Energy Spectra in Three-dimensional Low-β Magnetic

Reconnection. *Astrophysical Journal*, *884*(2), 118. doi: 10.3847/1538-4357/ab4268

Lin, J., Ko, Y.-K., Sui, L., Raymond, J. C., Stenborg, G. A., Jiang, Y., ... Mancuso, S. (2005, April). Direct Observations of the Magnetic Reconnection Site of an Eruption on 2003 November 18. *Astrophysical Journal*, *622*, 1251-1264. doi: 10.1086/428110

Lin, R. P., Krucker, S., Hurford, G. J., Smith, D. M., Hudson, H. S., Holman, G. D., ... Vilmer, N. (2003, October). RHESSI Observations of Particle Acceleration and Energy Release in an Intense Solar Gamma-Ray Line Flare. *Astrophysical Journal, Letters*, *595*, L69-L76. doi: 10.1086/378932

Loureiro, N. F., Cowley, S. C., Dorland, W. D., Haines, M. G., & Schekochihin, A. A. (2005, December). X-Point Collapse and Saturation in the Nonlinear Tearing Mode Reconnection. *Physical Review Letters*, *95*(23), 235003. doi: 10.1103/PhysRevLett.95.235003

Loureiro, Nuno F., & Boldyrev, Stanislav. (2017, June). Role of Magnetic Reconnection in Magnetohydrodynamic Turbulence. *Physical Review Letters*, *118*(24), 245101. doi: 10.1103/PhysRevLett.118.245101

Markidis, S., Lapenta, G., Divin, A., Goldman, M., Newman, D., & Andersson, L. (2012, March). Three dimensional density cavities in guide field collisionless magnetic reconnection. *Physics of Plasmas*, *19*(3), 032119. doi: 10.1063/1.3697976

Muñoz, P. A., & Büchner, J. (2016, October). Non-Maxwellian electron distribution functions due to self-generated turbulence in collisionless guide-field reconnection. *Physics of Plasmas*, *23*(10), 102103. doi: 10.1063/1.4963773

Ng, J., Egedal, J., Le, A., & Daughton, W. (2012). Phase space structure of the electron diffusion region in reconnection with weak guide fields. *Physics of Plasmas*, *19*(11), 112108. Retrieved from `https://doi.org/10.1063/1.4766895` doi: 10.1063/1.4766895

Ng, J., Egedal, J., Le, A., Daughton, W., & Chen, L.-J. (2011, Feb). Kinetic structure of the electron diffusion region in antiparallel magnetic reconnection. *Phys. Rev. Lett.*, *106*, 065002. Retrieved from `https://link.aps.org/doi/10.1103/PhysRevLett.106.065002` doi: 10.1103/PhysRevLett.106.065002

Nishizuka, N., Karlický, M., Janvier, M., & Bárta, M. (2015, February). Particle Acceleration in Plasmoid Ejections Derived from Radio Drifting Pulsating Structures. *Astrophysical Journal*, *799*, 126. doi: 10.1088/0004-637X/799/2/126

Øieroset, M., Lin, R. P., Phan, T. D., Larson, D. E., & Bale, S. D. (2002, Oct). Evidence for electron acceleration up to $\sim$ 300 keV in the magnetic reconnection diffusion region of earth's magnetotail. *Phys. Rev. Lett.*, *89*, 195001. Retrieved from `https://link.aps.org/doi/10.1103/PhysRevLett.89.195001` doi: 10.1103/PhysRevLett.89.195001

Øieroset, M., Phan, T. D., Fujimoto, M., Lin, R. P., & Lepping, R. P. (2001, July). In situ detection of collisionless reconnection in the Earth's magnetotail. *Nature*, *412*(6845), 414-417. doi: 10.1038/35086520

Oka, M., Phan, T.-D., Krucker, S., Fujimoto, M., & Shinohara, I. (2010, May). Electron Acceleration by Multi-Island Coalescence. *Astrophysical Journal*, *714*, 915-926. doi: 10.1088/0004-637X/714/1/915

Papadopoulos, K., & Palmadesso, P. (1976). Excitation of lower hybrid waves in a plasma by electron beams. *The Physics of Fluids*, *19*(4), 605-606. Retrieved from `https://aip.scitation.org/doi/abs/10.1063/1.861501` doi: 10.1063/1.861501

Phan, T. D., Bale, S. D., Eastwood, J. P., Lavraud, B., Drake, J. F., Oieroset, M., ... Velli, M. (2020, February). Parker Solar Probe In Situ Observations of Magnetic Reconnection Exhausts during Encounter 1. *Astrophysical Journal, Supplement*, *246*(2), 34. doi: 10.3847/1538-4365/ab55ee

Priest, E., & Forbes, T. (2000). *Magnetic Reconnection.* Cambridge University

Press, UK.

Pritchett, P. L., & Coroniti, F. V. (2004, January). Three-dimensional collisionless magnetic reconnection in the presence of a guide field. *Journal of Geophysical Research (Space Physics)*, *109*, A01220. doi: 10.1029/2003JA009999

Rogers, B. N., Drake, J. F., & Shay, M. A. (2000, October). The onset of turbulence in collisionless magnetic reconnection. *Geophysics Research Letters*, *27*(19), 3157-3160. doi: 10.1029/2000GL000038

Scholer, M., Sidorenko, I., Jaroschek, C. H., Treumann, R. A., & Zeiler, A. (2003). Onset of collisionless magnetic reconnection in thin current sheets: Three-dimensional particle simulations. *Physics of Plasmas*, *10*(9), 3521-3527. Retrieved from `https://doi.org/10.1063/1.1597494` doi: 10.1063/1.1597494

Shay, M. A., Phan, T. D., Haggerty, C. C., Fujimoto, M., Drake, J. F., Malakit, K., ... Swisdak, M. (2016). Kinetic signatures of the region surrounding the x line in asymmetric (magnetopause) reconnection. *Geophysical Research Letters*, *43*(9), 4145-4154. Retrieved from `https://agupubs.onlinelibrary.wiley.com/doi/abs/10.1002/2016GL069034` doi: 10.1002/2016GL069034

Silin, I., & Büchner, J. (2006, January). Three-dimensional Vlasov-code simulations of magnetopause-like current sheets. *Advances in Space Research*, *37*(7), 1354-1362. doi: 10.1016/j.asr.2005.05.025

Sironi, L., & Spitkovsky, A. (2014, Mar). Relativistic Reconnection: An Efficient Source of Non-thermal Particles. *Astrophysical Journal, Letters*, *783*(1), L21. doi: 10.1088/2041-8205/783/1/L21

Siversky, T. V., & Zharkova, V. V. (2009, October). Particle acceleration in a reconnecting current sheet: PIC simulation. *Journal of Plasma Physics*, *75*, 619-636. doi: 10.1017/S0022377809008009

Somov, B. V. (Ed.). (2000). *Cosmic Plasma Physics* (Vol. 251). doi: 10.1007/978-94-015-9592-6

Song, H.-Q., Chen, Y., Li, G., Kong, X.-L., & Feng, S.-W. (2012, April). Coalescence of Macroscopic Magnetic Islands and Electron Acceleration from STEREO Observation. *Physical Review X*, *2*(2), 021015. doi: 10.1103/PhysRevX.2.021015

Takasao, S., Asai, A., Isobe, H., & Shibata, K. (2012, January). Simultaneous Observation of Reconnection Inflow and Outflow Associated with the 2010 August 18 Solar Flare. *Astrophysical Journal, Letters*, *745*, L6. doi: 10.1088/2041-8205/745/1/L6

Verboncoeur, J. P., Langdon, A. B., & Gladd, N. T. (1995, May). An object-oriented electromagnetic PIC code. *Computer Physics Communications*, *87*, 199-211. doi: 10.1016/0010-4655(94)00173-Y

Vilmer, N., MacKinnon, A. L., & Hurford, G. J. (2011, September). Properties of Energetic Ions in the Solar Atmosphere from γ-Ray and Neutron Observations. *Space Science Reviews*, *159*, 167-224. doi: 10.1007/s11214-010-9728-x

Wang, R., Lu, Q., Nakamura, R., Huang, C., Du, A., Guo, F., ... Wang, S. (2016, 3 1). Coalescence of magnetic flux ropes in the ion diffusion region of magnetic reconnection. *Nature Physics*, *12*(3), 263–267. doi: 10.1038/nphys3578

Wang, S., Chen, L.-J., Bessho, N., Kistler, L. M., Shuster, J. R., & Guo, R. (2016). Electron heating in the exhaust of magnetic reconnection with negligible guide field. *Journal of Geophysical Research: Space Physics*, *121*(3), 2104-2130. Retrieved from `https://agupubs.onlinelibrary.wiley.com/doi/abs/10.1002/2015JA021892` doi: 10.1002/2015JA021892

Xia, Q., & Zharkova, V. (2020, March). Particle acceleration in coalescent and squashed magnetic islands II. Particle-in-cell approach. *Astronomy and Astrophysics*, *635*, A116.

Zank, G. P., le Roux, J. A., Webb, G. M., Dosch, A., & Khabarova, O. (2014, December). Particle Acceleration via Reconnection Processes in the Supersonic Solar Wind. *Astrophysical Journal*, *797*, 28. doi: 10.1088/0004-637X/797/1/

28

Zenitani, S., & Hoshino, M. (2008, April). The Role of the Guide Field in Relativistic Pair Plasma Reconnection. *Astrophysical Journal*, *677*(1), 530-544. doi: 10.1086/528708

Zhang, Q., Drake, J. F., & Swisdak, M. (2019). Instabilities and turbulence in low-guide field reconnection exhausts with kinetic riemann simulations. *Physics of Plasmas*, *26*(10), 102115. Retrieved from `https://doi.org/10.1063/1.5121782` doi: 10.1063/1.5121782

Zharkova, V., & Khabarova, O. (2015, April). Additional acceleration of solar-wind particles in current sheets of the heliosphere. *Annales Geophysicae*, *33*, 457-470. doi: 10.5194/angeo-33-457-2015

Zharkova, V. V., & Agapitov, O. V. (2009, April). The effect of magnetic topology on particle acceleration in a three-dimensional reconnecting current sheet: a test-particle approach. *Journal of Plasma Physics*, *75*, 159-181. doi: 10.1017/S002237780800771X

Zharkova, V. V., Arzner, K., Benz, A. O., Browning, P., Dauphin, C., Emslie, A. G., ... Vlahos, L. (2011, September). Recent Advances in Understanding Particle Acceleration Processes in Solar Flares. *Space Science Reviews*, *159*, 357-420. doi: 10.1007/s11214-011-9803-y

Zharkova, V. V., & Gordovskyy, M. (2004, April). Particle Acceleration Asymmetry in a Reconnecting Nonneutral Current Sheet. *Astrophysical Journal*, *604*, 884-891. doi: 10.1086/381966

Zharkova, V. V., & Gordovskyy, M. (2005, January). Energy spectra of particles accelerated in a reconnecting current sheet with the guiding magnetic field. *Monthly Notices of the RAS*, *356*, 1107-1116. doi: 10.1111/j.1365-2966.2004.08532.x

Zharkova, V. V., & Khabarova, O. V. (2012, June). Particle Dynamics in the Reconnecting Heliospheric Current Sheet: Solar Wind Data versus Three-dimensional Particle-in-cell Simulations. *Astrophysical Journal*, *752*, 35. doi: 10.1088/0004-637X/752/1/35

Zhong, J. Y., Lin, J., Li, Y. T., Wang, X., Li, Y., Zhang, K., ... Zhang, J. (2016). Relativistic electrons produced by reconnecting electric fields in a laser-driven bench-top solar flare. *The Astrophysical Journal Supplement Series*, *225*(2), 30. Retrieved from `http://stacks.iop.org/0067-0049/225/i=2/a=30`

Zhou, M., Li, H., Deng, X., Huang, S., Pang, Y., Yuan, Z., ... Tang, R. (2014). Characteristic distribution and possible roles of waves around the lower hybrid frequency in the magnetotail reconnection region. *Journal of Geophysical Research: Space Physics*, *119*(10), 8228-8242. Retrieved from `https://agupubs.onlinelibrary.wiley.com/doi/abs/10.1002/2014JA019978` doi: 10.1002/2014JA019978

Zong, Q.-G., Fritz, T. A., Pu, Z. Y., Fu, S. Y., Baker, D. N., Zhang, H., ... Reme, H. (2004, September). Cluster observations of earthward flowing plasmoid in the tail. *Geophysics Research Letters*, *31*, L18803. doi: 10.1029/2004GL020692